Sensors & Transducers

Infrared Thermal Signature Evaluation of a Pure and Saline Ice for Marine Operations in Cold Climate

[1] Taimur Rashid, Hassan A. Khawaja, K. Edvardsen, [2] Umair N. Mughal

[1] Department of Engineering and Safety, Arctic University of Norway (UIT), 9019, Tromsø, Norway
[2] Department of Industrial Engineering, Narvik University College (HIN), 8505, Narvik, Norway
[1] Tel.: +47 98984712
[1] taimur.rashid@uit.no:

Abstract: Marine operations in cold climates are subjected to abundant ice accretion, which can lead to heavy ice loads over larger surface area. For safe and adequate operations on marine vessels over a larger area, remote ice detection and ice mitigation system can be useful. To study this remote ice detection option, lab experimentation was performed to detect the thermal gradient of ice with the infrared camera. Two different samples of ice blocks were prepared from tap water and saline water collected from the North Atlantic Ocean stream. The surfaces of ice samples were observed at room temperature. A complete thermal signature over the surface area was detected and recorded until the meltdown process was completed. Different temperature profiles for saline and pure ice samples were observed, which were kept under similar conditions. This article is focused to understand the experimentation methodology and thermal signatures of samples. However, challenges remains in terms of the validation of the detection signature and elimination of false detection.

Keywords: Icing; infrared; thermal signature; cold region; saline ice.

---

1. Introduction

Ice accretion problems are challenging in the cold climate regions. With a rise in activity in the arctic frontier, icing phenomena will increasingly affect operational activities. The sources of icing may vary according to environmental conditions, for instance atmospheric icing (snow, rain, fog) [1] or sea spray icing generated due to wind or wave-structure collision [2]. In marine icing events, combination of the mentioned causes could also be the case. An example of this is the snow that sticks to a wet surface caused by the sea spray. All of the discussed factors can cause heavy ice accumulation on offshore and mobile platforms operating in the cold climates [3]. Adequate measures are required to minimize the influence of atmospheric and sea spray icing events on structures under different conditions and, therefore, effective anti/de-icing techniques become important [4]. These techniques involve thermal, chemical and mechanical methods to avoid and/or remove the ice [5]. Most often the problem arises in situations where unpredicted or unexpected environmental conditions occur that could cause heavy ice accretion phenomena, as the ice accretion rate is high enough to become a possible threat to the structure. In such cases the time elapsed becomes the critical factor in responding in an effective manner, which also includes ice mitigation and removal. A viable option available is timely ice detection over the structure during heavy icing events, which should

support the anti/de-icing systems. Timely detection can be important to the mitigation of heavy ice loads upon structures.

This paper is a continuation of the experimenetation process to evaluate thermal infrared (IR) signature of the icing surface [6]. A brief insight into the concept of infrared (IR) thermography is given in Section II. Suitable wavelengths to detect cold obects with infrared detectors is also discussed. Section III gives the details about experimentation performed to evaluate the IR thermal signature of a pure and saline ice block and the results are discussed in Section IV. Also included is a brief discussion on remote IR detection in marine operations, which will be the applicability of this research project followed by the concluding remarks in Section V.

2. IR Thermography and Thermal Signature Detection at Low Temperatures

IR light is electromagnetic radiation with a wavelength longer than that of visible light, measured from the nominal edge of visible red light at $0.74\mu m$ and extending conventionally up to $300\mu m$. Figure 1 shows the IR spectral band that is generally sub-divided into four sub-bands; near infrared (NIR) ranges between $0.75-1\mu m$, shortwave infrared (SWIR) is from $1-2.5~\mu m$, middle infrared (MWIR) is between $3-5\mu m$, longwave infrared (LWIR) is between $8-14\mu m$.
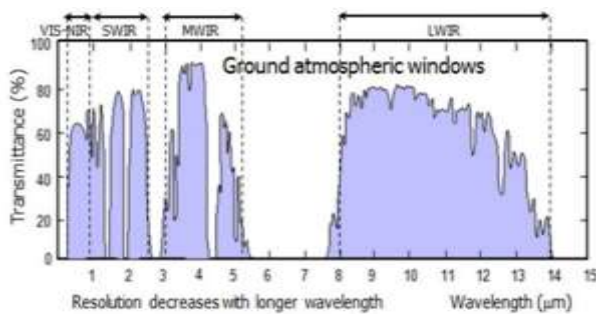

Fig. 1. IR Spectrum **[7]**

For cold objects near 0°C, the prominent radiation wavelength is near 11 µm. Since most commercial IR sensors use wavelengths between 8 to 14 µm, IR thermography can be handful for surface ice studies [8]. Theoretically, each body at any temperature above absolute zero will emit some radiation, but the intensity and frequency distribution of the radiation is different based on the basic structure of the body. The energy emitted by a true blackbody is the maximum theoretically possible for a given temperature. The radiative power (or number of photons emitted) and its wavelength distribution are given by the Planck's

radiation law (given by (1) and (2)), where λ is the wavelength, T is the temperature, h is Planck's constant, c is the velocity of light, and k is Boltzmann's constant.

$$\frac{2\pi hc^2}{\lambda^5}[\exp(\frac{hc}{\lambda KT})-1]^{-1}W/(cm^2\mu m) \qquad (1)$$

$$P(\lambda,T) = \frac{2\pi c}{\lambda^4}[\exp(\frac{hc}{\lambda KT})-1]^{-1}photons/(scm^2\mu m) \qquad (2)$$

Figure 2 shows a plot of these curves for a number of blackbody temperatures. With a rise in temperature, the energy emission at any given wavelength increases respectively and the wavelength of peak emission decreases, which is specified by Wien's displacement law. The waveband 1–15 µm in the IR region of the electromagnetic spectrum contains the maximum radiative emission for thermal imaging purposes.
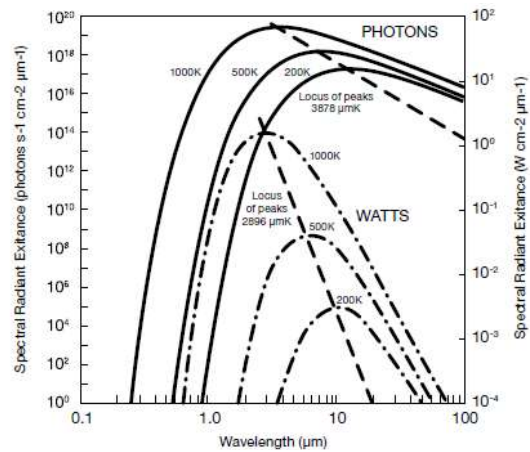

Fig. 2. Spectral radiance excitance (Planck's Law) **[9]**

The working principle of an IR camera is based on thermography imaging. The major components of the camera are lens, detector, video processing electronics and user interface control. The incident beam of light is focused by the lens upon the detector. The detector contains the IR sensitive elements arranged in the array called focal plane array (FPA). These are IR sensitive elements and miniature in size (micro-meters). The resolution of FPA determines the resolution of the IR imagery produced by the camera. Many IR cameras available have user interface to calculate the scene temperature along with imagery recording software. Calibration is often required to read out the correct temperature across the scene that is captured.

With the advancement in the IR camera-technology, significant work has been done to observe ice/snow emissive properties to support remote microwave detection. Snow and clear ice have high emissivity values, which makes them convenient to thermally image. Snow emissivity has been variously found to be 0.98 for frost [10],

above 0.98 for small-grained snow under 1000 μm [11], 0.96 for flat solid ice and water, and as low as 0.8 for old snow. Measurements obtained at particular wavelengths (e.g. 10 μm) have observed emissivity as high as 0.995. Conversely, the thermal reflectance of snow *r* is less than 2.3% between the 4 to 14 μm wavelengths [12]. This holds good for various snow types including granular, fine, wet, and dry; whereas newly fallen snow reflectance is less than 1% between 4 to 14μm. For most of the 7.5 to 13μm spectrum, the emissivity is found higher in comparison. Therefore, IR cameras operating in the range above 7.5μm can prove significant to observe cold objects.

3. Pure and Saline Ice Thermal Profiles and Signatures

3.1. Experimental Setup

In order to test the potential of IR ice detection, it is necessary to evaluate the thermal signature of icing. To detect the IR signature of pure ice, basic lab experimentation was performed. The pure ice sample was prepared in a container from freezing tap water in a commercial freezer. The dimension of the ice block prepared was 14.5 x 14 x 5.5 cm. Although the dimensions were randomly chosen, it was taken into consideration that the ice block should have a large enough surface area to allow observation of a differentiating thermal signature and a wide range of temperature profiles. As a starting point, the viewing angle of the IR camera and the ice sample was kept at 90 degrees. The forward-looking IR camera FLIR A310 was used to observe the thermal signature of the block using the proprietary software of the FLIR device. The observations acquired were produced in the mentioned calibrated software. FLIR A310 series IR camera has a detector operating in the range of MWIR (8-11μm). The thermal signature was recorded immediately from the time when sample was taken out of the freezer. The observations were recorded until the melt-down phenomena had started at room temperature and surface of the ice block acquired a uniform temperature.

The lab setup performed is shown in the Figure 3. An attempt was made to observe a freely suspended ice block in order to ensure the uniform heat transfer from all directions. To hold the ice block on the stand, a wooden piece was immersed into the cold water during freezing process, so that it could be used as a suspension support assisted by a clamping stand as shown in Figure 3. Minimal thermal conduction from the ice block was expected from the wooden support (since the wood

has poor conductivity), apart from fulfilling the suspension support requirement. The ice block was initially frozen to approximate -26°C, suspended on the stand immediately after taking out of the freezer and observed from IR camera. FLIR A310 has an uncooled detector device that sends IR frames processed at the rate of 5Hz. The FLIR calibrated software acquires the frames and saves them as a sequence file. The camera to software communication is performed via an Ethernet protocol. The IR image of the larger surface-1 and relatively smaller surface-2 (Figure 3) was recorded at room temperature to evaluate the surface temperature profiles.
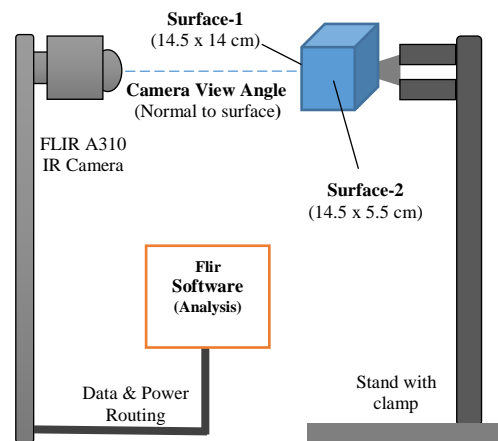

Fig. 3. **L**ab setup of pure ice block thermal signature evaluation

3.2. Pure Ice Testing Results

The temperature observations were made along a linear path along the ice block's center line to capture the maximum thermal gradient across the surface. This helped to acquire the maximum and minimum temperature profiles over the surfaces 1, 2 (Figure 4). Minimum temperatures of -26.5°C for surface-1 and -23.7°C for surface-2 were recorded. The gradual rise in temperature for both the surfaces was observed simultaneously as the heat transfer process took place at room temperature. The observations for surface-1 are noted after regular intervals of time t0 to t0+32 and also simultaneously for surface-2 as shown in Figure 4. The thermal IR signature available from the camera optics was captured during the course of the observations, which presents the distribution of the thermal profile as shown in Figure 5. The lowest temperature profile was observed almost at the center of the ice block surfaces whereas the maximum temperature at the boundaries.
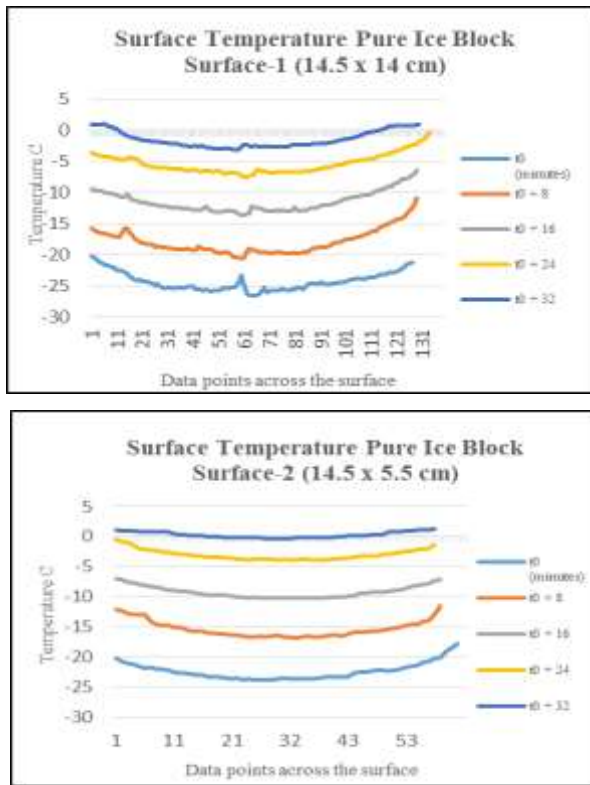
Fig. 4. Surface temperature of Ice block recorded from thermal IR signature at different intervals
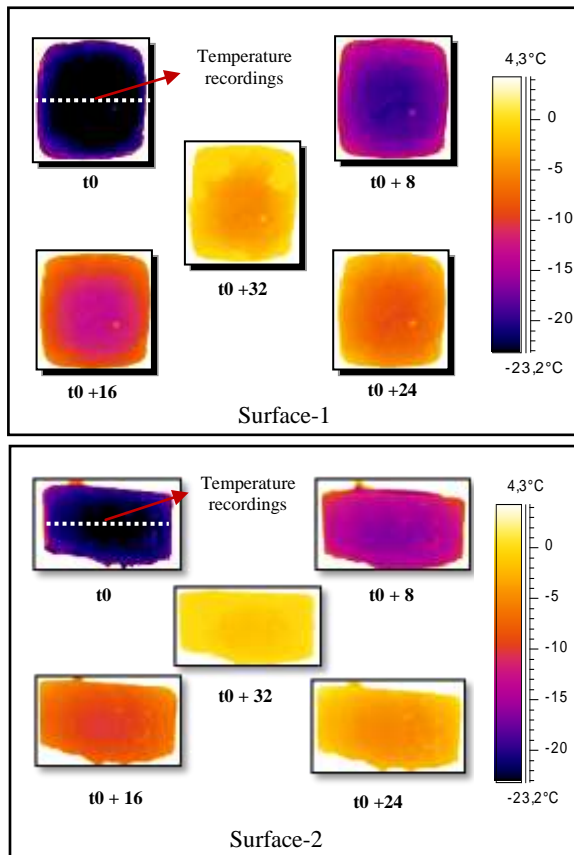

Fig. 5. Images of pure ice block recorded from thermal IR signature at different intervals until meltdown

3.2. Pure and Saline Ice Block Comparison

In addition to pure ice, the saline ice block temperature profile and thermal signature was also observed. The saline water used for the experimentation was collected from the North Atlantic Ocean stream in Tromsø, Norway. The saline ice sample was prepared in a similar manner as described in Section 3.1. To make a comparison of pure and saline ice, both samples were prepared in similar conditions and each sample's surface was observed simultaneously at room temperature. These observations were recorded from the time both samples were taken out of the freezer. It was observed that both samples were at different temperatures from the starting time (t0) of temperature recordings. The observations were recorded at a linear path along the central line of the icing surface at t0, t0+20, t0+30, t0+40 (minutes) until the pure ice acquired uniform temperature. The experimentation was continued for the saline ice block and observations were recorded at t0+60, t0+70, t0+80 and t0+90(minutes).
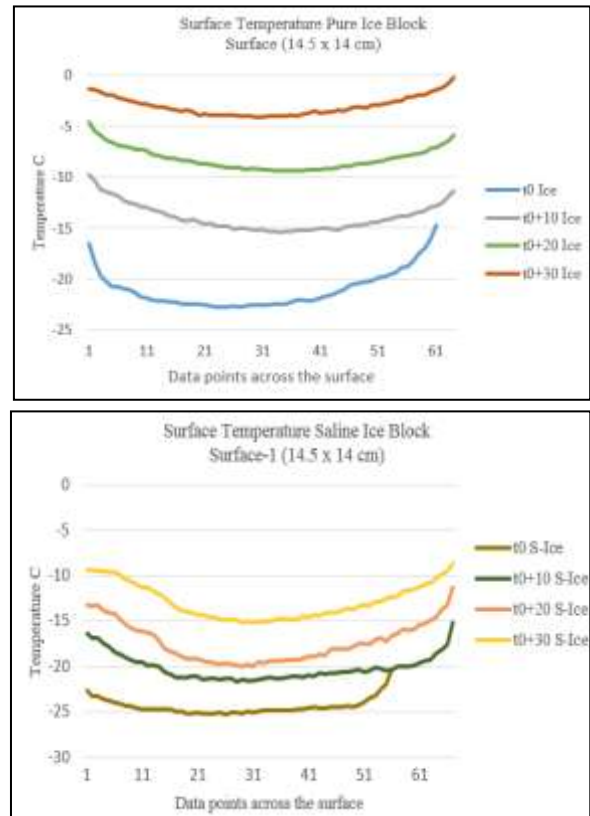

Fig. 6. Surface temperature profiles of Pure and Saline Ice block simultaneously observed from IR image under similar conditions

Difference in the temperatures was observed from the start of the recordings and saline ice block was at the lower temperature of -25°C as compared

4

to the -22°C of pure ice as shown in figure 6. Figure 6 also shows the temperature profiles of both ice samples observed at different periods. The corresponding IR iso-thermal signature is shown is figure 8. It was observed that the pure ice block melted down earlier at approximately t0+40 minutes. The saline ice continued to show the varying temperature profile for approximately t0+95 minutes. It was observed that on the saline ice surface, saline water droplets started to drain from the period of t0+10 minutes. These saline droplets continued to drain at a slower pace from the boundary of suspended saline ice block. One the other hand, water droplets were not observed on the pure ice surface until it reached the melting point.

4. Discussion

Ice has a high emissive value and it produces a distinguishable thermal signature shown in Figure 5 and Figure 8. The pure ice block suspended through the wooden stick allowed the ice to conduct heat uniformly. The IR observations show the thermal gradient from the center of the ice block towards the outside, which follows the heat transfer process. The heat conduction through the boundary layer of the pure ice can be easily identified from the thermal signatures as shown in Figure 5. The minimum temperature at surface-1 is -26.5°C at t0 (Figure 4), which is located in the geometric center of the surface. A similar behavior is observed at surface-2 of pure ice sample. In terms of the maximum temperature profile at the boundary layers, not much difference was observed between both the surfaces of pure ice block. The highest temperature of 0.92°C was observed at the boundary of surface-1 at t0 as compared to the 1.1°C of surface-2 shown in Figure 4. The maximum-minimum difference in the two surface areas was noted as surface-1 has wider span of temperature range as compared to the surface-2 possibly because of the larger surface area. The maximum-minimum temperature difference at time t0 to t0+32 for surface-1 was 6.44°C, 9.61°C, 7.32°C, 6.98°C and 4.07°C respectively. At similar time intervals (t0 to t0+32) for surface-2, the difference between maximum and minimum temperature recorded was 5.99°C, 5.24°C, 3.2°C, 3.2°C and 1.59°C. The temperature profiles of the pure ice block can be correlated with the isothermal images shown in the Figure 5. In the IR image of both the ice surfaces, the difference in thermal signature can also be observed at the boundary layer of the ice block, which is at a higher temperature as compared to the rest of the surface block. The temperature profile decreases from corners to the center of the ice block. Since the room temperature was uniform throughout the experiment, it can be safely said that maximum heat transfer occurred from the boundary through natural convection.

In the comparison part of experimentation process, the surfaces of saline ice and pure ice were found to be at different freezing temperatures when taken out of the freezer. The difference in the temperature profiles was evident during the experimentation process as shown in Figure 6. If we compare the temperature ranges for these icing types, it can be observed that the saline ice at room temperature remained at lower temperature. Figure 7 shows the percentile area of temperature profiles observed at t0, t0+20 and t0+40 minutes.
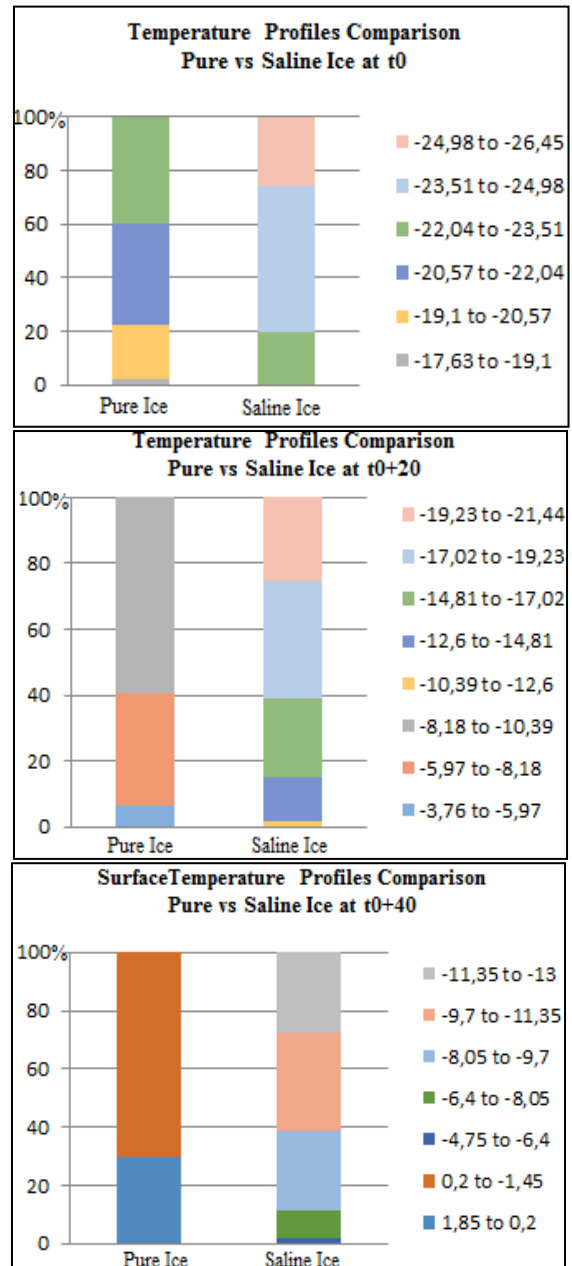

Fig. 7. Surface temperature profiles of pure and saline ice block simultaneously observed from IR Camera

Initially at t0, a large surface area (60%) of saline ice was at the temperature between -23.5°C to -25°C whereas pure ice was distributed between -22°C to -23.5°C (40% area) and -20.5°C to -22°C

(40% area). At the mid-time interval before pure was ice melted (i.e. at t0+20 minutes), major area of pure ice (60%) was between -8.1°C to -10.3°C whereas saline ice had approximately evenly distributed temperature on its surface between -19°C to -10°C (Figure 7). After t0+40 minutes, the pure ice melted and majority of its surface area had a temperature between -1.45°C to 0.2°C (Figure 7). The saline ice steadily melted until t0+95 minutes showing various temperature profiles. The rest of the temperature ranges for saline ice block after time period t0+40 minutes are shown in Figure 9. The difference in surface temperatures observed for the saline ice block reduced in the latter half of the experimentation. The temperature range available on the saline ice block after t0+50 minutes was between 3.8°C to 4.5°C for each time of the recordings as shown in Figure 10.
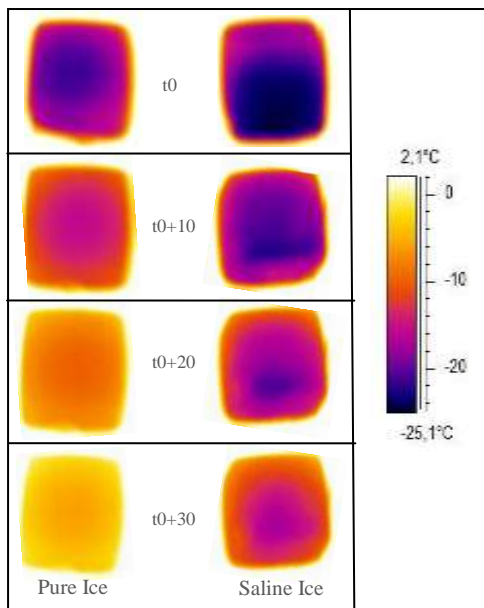

Fig. 8. Images of pure and saline ice blocks from thermal IR signature recorded under similar conditions
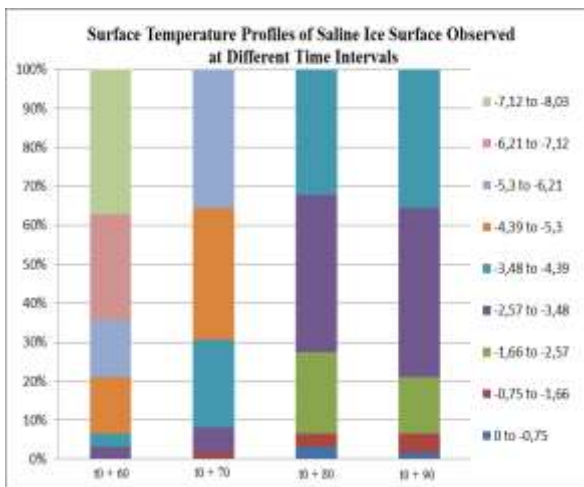

Fig. 9. Surface temperature profiles of saline ice block for rest of the time period (t0+60 onwards)

Figure 10 also shows the comparison of differences between maximum and minimum absolute temperature recordings at the period specified above. The saline ice showed wider range of temperature as compared to pure ice during the time period t0+10 to t0+40 minutes as shown in Figure 10. At the start of experimentation, the absolute temperature difference between both icing surfaces (pure and saline) was at the same level (8°C to 9°C), but for pure ice it reduced considerably. On the other hand, steady decline in the absolute temperature difference is evident for the saline ice as shown in Figure 10. It shows the steady heat conduction process as compared to pure ice block. It is to be noted that the salinity factor is contributing towards steady decline in temperature of saline ice (Figure 10). The salinity of ice accreted upon structures during the marine icing phenomenon might vary with the contributing environmental factors. This can affect the conduction process and eventually contribute to various temperature profiles observed from IR camera.
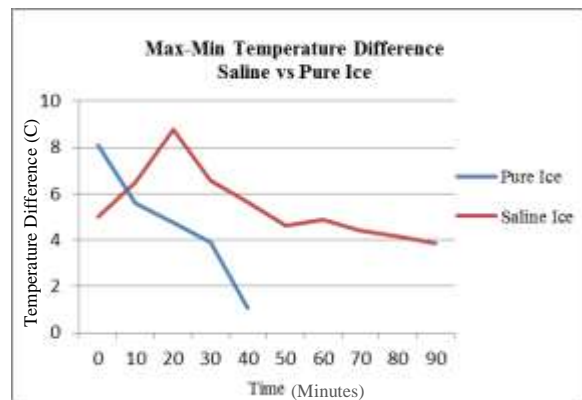

Fig. 10. Absolute maximum and minimum temperature difference (Saline vs Pure Ice)

Overall, the wide range of the IR thermal profile was available for pure and especially saline ice block (Figure 4, 6, 7 and 9). This also assisted in differentiating it with a relatively hotter environment during the experimentation process, though in a cold climate environment this may not be the scenario. IR detection for colder objects seems to works well as long as thermal non-uniformity is present in the scene which is to be observed. Currently, offshore structures and marine ships operating in cold environment use thermal methods for anti/de-icing, apart from other methods. Thermally active heated floors will generate a predictable IR signature. Ice accretion on the floors may result in different thermal signature. This variation may be used for ice detection and may also lead to the detection of the ice accretion rate if used in conjunction with heat transfer theory.

5. Conclusion

The thermal signature of icing can be applied to detect cold objects especially on ice accreted upon the structures using IR camera. The lab experimentation of pure and saline ice block shows the thermal signature and gradient of these surface areas. Different temperature profiles were noticed for saline and pure ice, which were kept under similar conditions. The saline ice showed steady heat conduction process at room temperature as compared to pure ice, which melted down earlier and acquired uniform temperature less than half of the time taken by saline ice. Wide range of thermal profiles from absolute temperature of 4°C to 9°C was observed from the infrared detector. Study of IR observation of ice block showed that temperature varies over time with maximum value at the boundaries and minimum at the center. The difference between the boundary and the center temperature is higher on a larger surface area. The influence of emissivity values on ice detection is not discussed in this study. The experimentation conducted is based on passive IR detection of ice block. If any object having same emissivity as of ice is captured in the IR scene, false detection of ice can be the challenge. Further modifications are needed in that scenario to make the ice detection reliable and to avoid false detection. The introduction of active heating mechanism underneath the icing surface can be one of the options. This can assist to distinguish the thermal IR signature of ice based on its conductive properties. The discussed option can lead to advanced experimentation specifically designed for cold regions and marine arctic operations to validate the ice detection and growth.

Acknowledgements

References

1. S. Fikke, et al., Cost 727: atmospheric icing on structures. Measurements and data collection on icing: State of the Art, Publication of MeteoSwiss, 2006. 75(110): p. 1422-1381.
2. L. Makkonen, Salinity and growth rate of ice formed by sea spray. Cold Regions Science and Technology, 1987. 14(2): p. 163-171.
3. C.C. Ryerson, Ice protection of offshore platforms. Cold Regions Science and Technology, 2011. 65(1): p. 97-110.
4. M. Farzaneh, and C.C. Ryerson, Anti-icing and deicing techniques. Cold Regions Science and Technology, 2011. 65(1): p. 1-4.
5. C.C. Ryerson, Icing Management for Coast Guard Assets. 2013, Engineering Research and Development Center, Cold regions research and engineering lab: Hanover NH.
6. T. Rashid, H.A.K., K. Edvardsen, U.N. Mughal, Infrared Thermal Signature Evaluation of a Pure Ice Block, in International Conference on Sensor Technologies and Applications (SENSORCOMM). 2015: Italy. p. 119.
7. N.K. Dhar, R. Dat, and A.K. Sood, Advances in Infrared Detector Array Technology. Optoelectronics - Advanced Materials and Devices. 2013.
8. W.G Rees, Remote sensing of snow and ice. 2005: CRC Press.
9. A. Rogalski, Infrared detectors: an overview. Infrared Physics & Technology, 2002. 43(3): p. 187-210.
10. W.L. Wolfe, and G.J. Zissis, The infrared handbook. Arlington: Office of Naval Research, Department of the Navy, 1978, edited by Wolfe, William L.; Zissis, George J., 1978. 1.
11. J. Dozier, and S.G. Warren, Effect of viewing angle on the infrared brightness temperature of snow. Water Resources Research, 1982. 18(5): p. 1424-1434.
12. J.W. Salisbury, D.M. D'Aria, and A. Wald, Measurements of thermal infrared spectral reflectance of frost, snow, and ice. Journal of Geophysical Research: Solid Earth (1978–2012), 1994. 99(B12): p. 24235-24240.